

Article

Enhancement of the Young's Modulus through Infrared Heat Treatment: A Study of the Microstructure and the Mass Effect of Real Body 6082 Aluminum Forgings

Yi-Ling Chang , Fei-Yi Hung *  and Truan-Sheng Lui

Department of Materials Science and Engineering, National Cheng Kung University, Tainan 70101, Taiwan; lingiscute@gmail.com (Y.-L.C.); luits@mail.ncku.edu.tw (T.-S.L.)

* Correspondence: fyhung@mail.ncku.edu.tw; Tel.: +886-6-275-7575 (ext. 62950)

Received: 9 March 2018; Accepted: 4 April 2018; Published: 4 April 2018



Abstract: To avoid the phenomenon of abnormal grain coarsening, and increase the Young's modulus of forgings, an infrared heat treatment was used on different mass forgings and compared with the results of an air furnace heat treatment. This work focused on the effects of microstructural evolution and the mechanical properties of two different mass 6082 real forgings. The experimental results show that infrared heat treatment can effectively reduce the mass effect after heat treatment, inhibit the coarse grains formed, and keep the non-equiaxed grains along the metal flows, thus significantly improving the ductility of the material. In addition, the rapid heating characteristic of infrared can effectively shorten the duration of heat treatment and greatly enhance the Young's modulus and the vibration resistance of 6082 entity forgings.

Keywords: 6082 aluminum alloy; forging; infrared heating; mechanical property; Young's modulus

1. Introduction

The 6082 alloy investigated is part of the AA6xxx (Al-Mg-Si) series of aluminum alloys. Their characteristics include light weight, high workability, strength properties, and corrosion resistance [1]; hence, they have been widely used in the automotive industry, for example, in automobile suspension components.

Most automobile suspension components are manufactured using a high temperature forging process [2,3]. The alloy forging process is conducted with an extruded bar and the use of pressure to shape it into the required form under a set temperature condition. During the forging process, the microstructure and the strength of the alloy changes, and the mechanical properties are improved [4]. Among them, the heat treatable 6082 aluminum alloy can be used with a subsequent heat treatment to achieve the desired mechanical material properties [5]; therefore, the heat treatment process is quite important in the 6082 forging process. Additionally, the effect of heat treatment on 6082 aluminum alloy forgings with different mass is also of importance.

Nowadays, according to previous studies, the coarse grain formed during the forming process can easily become coarser after the air furnace solution treatment process, which has been a thorny problem and has greatly affected the development of the 6082 aluminum alloy forging industry [2,3]. Grain coarsening is affected by the heat treatment time and temperature; hence, an infrared (IR) heat treatment was used in this study.

Compared to the air furnace heating method, the advantages of Infrared (IR) heat treatment are that it is convenient, cheap, energy saving, high penetration, has a short heating up period, and the temperature is easy to control [6]. It has been reported that using the IR heat treatment could preheat

billets rapidly [7] and may shorten the duration of solution treatment of AA2618 and AA6061 [6,8], and our team also reported that IR heat treatment could be used to heat 6082 aluminum cast-forging parts [9]. Therefore, in this study, it is expected that the solution heat treatment and precipitation aging process can be completed in a short duration through the high penetration efficacy and short heating up characteristics of infrared heat treatment. This study also evaluates the effects of mechanical properties corresponding to the same heat treatment of different masses.

Young's modulus was calculated after the heat treatments. A higher Young's modulus results in better workability and enhances the thinning potential; hence, a higher Young's modulus has a great significance for the use of 6082 forgings. Xie et al. [10] reported that the Young's modulus of the 6082 aluminum alloy increases after the aging process. In addition, Reeb et al. [11] also reported that the Young's modulus increased after the aging process; however, the improvement was not shown to be significant. Furthermore, based on our previous research [12], rapid heat solutionizing can increase the solid solution concentration (Mg, Si atoms) and provide improved precipitation benefits; hence, the Young's modulus after an IR heat treatment is calculated to put forward data for the application of 6082 forgings with high vibration resistance.

Here, we present an investigation of the influence of IR heat treatment regimens with different masses on 6082 forgings. The findings regarding the mass effect and microstructure, respectively, and their contribution to mechanical properties are an attempt to lead to a better understanding of and improvement in heat treatments following the 6082 aluminum alloy forging process.

2. Materials and Experimental Process

High temperature (500 °C) forged 6082 aluminum forgings were used in this study. The chemical composition of the forgings is given in Table 1. An IR heat treatment was used to clarify the property differences between 6082 forgings (L and S) with two different masses. Large forgings (L) were made from 60 mm diameter extruded bars, for which the size was 542 mm (l) \times 50~90 mm (w) \times 30 mm (h), and the weight was 1.68 kg. The small ones (S) were made from 35 mm diameter extruded bars, for which the size was 224 mm (l) \times 23~43 mm (w) \times 22~35 mm (h), and the weight was 0.24 kg, as shown in Figure 1.

Table 1. Chemical composition (wt. %) of a 6082 aluminum alloy.

Element	Mg	Si	Cu	Mn	Cr	Fe	Al
wt. %	0.97	1.2	0.06	0.86	0.16	0.18	Bal.

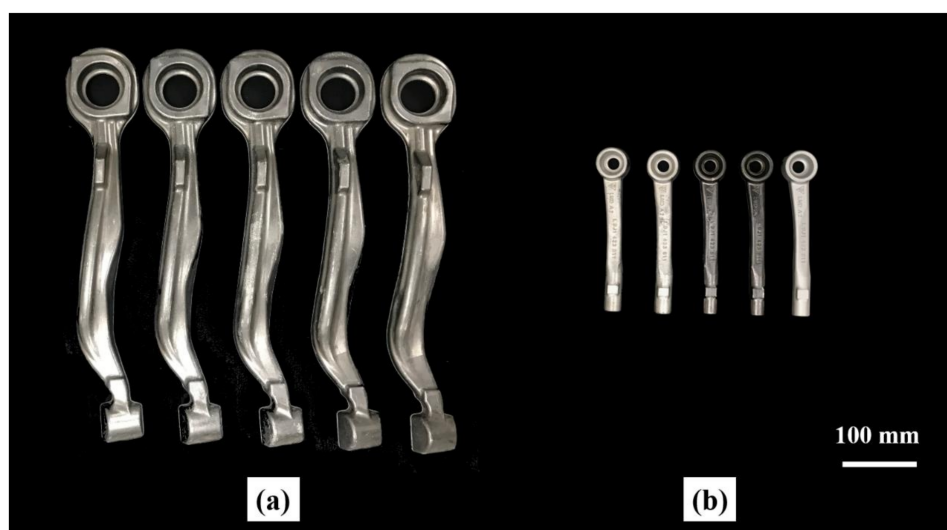


Figure 1. Photograph of the 6082 aluminum forgings: (a) Large forgings (L), (b) Small forgings (S).

According to our previous experimental results and previous research [2,13], the solution treatment condition for air furnace should be under 530 °C/4 h or grain would grow, hence, 525 °C/1 h was chosen as the air furnace heat treatment temperature and times for S forging (SAir). On the other hand, to make sure the L forgings can be fully solutionized in the air furnace, 540 °C/2 h was chosen as the L forging experiment parameters (LAir), whereas, due to the high penetration of IR, the solution treatment could be done in 30 min. at 560 °C. The specimen codes for all experiments are shown in Table 2.

Table 2. Experimental parameters and specimen codes.

Sample Condition	Solution Treatment	Artificial Aging	Code
Forging L	Air, 540 °C, 2 h	Air, 175 °C, 2 h	LAir
	IR, 560 °C, 30 min.	IR, 180 °C, 6 h	L180-6H
	IR, 560 °C, 30 min.	IR, 190 °C, 1 h	L190-1H
	IR, 560 °C, 30 min.	IR, 190 °C, 2 h	L190-2H
Forging S	Air, 525 °C, 1 h	Air, 175 °C, 6 h	SAir
	IR, 560 °C, 30 min.	IR, 180 °C, 6 h	S180-6H
	IR, 560 °C, 30 min.	IR, 190 °C, 1 h	S190-1H
	IR, 560 °C, 30 min.	IR, 190 °C, 2 h	S190-2H

The microstructure observation and the hardness test sample sampling location are shown in Figure 2. The microstructure and the second phases of the alloy after heat treatment were observed using optical microscopy (OM, OLYMPUS BX41M-LED, OLYMPUS, Tokyo, Japan), Scanning electron microscope (SEM, SU-5000, HITACHI, Tokyo, Japan,) equipped with an energy dispersive spectrometer (EDS, EDAX, Singapore, Singapore) and X-ray diffraction (XRD, Bruker AXS GmbH, Karlsruhe, Germany). For the OM observations, the samples were ground using SiC papers from #120 to #4000, and polished in an Al₂O₃ aqueous suspension (1.0 and 0.3 μm) and an SiO₂ polishing suspension and then etched (using Keller's reagent and KMnO₄ (Taiwan Green Version Technology Ltd., Taipei, Taiwan)). The XRD patterns were recorded when Cu Kα radiation was employed from 2θ = 10–60° to identify the intermetallic compounds. Hardness measurements were performed on heat treated samples and were evaluated using the Rockwell hardness (HR) test (Mitutoyo, Kawasaki-shi, Japan). The measurement conditions for the HR test followed the B-scale, and the mean value for five impressions was taken as the hardness of the corresponding condition.

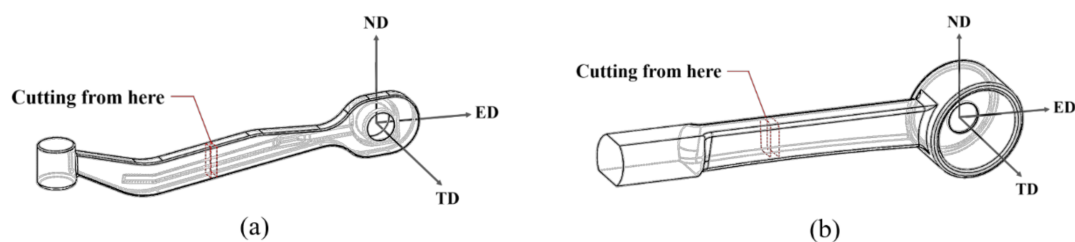


Figure 2. Diagram of microstructure and hardness test specimens: (a) L, (b) S.

Tensile tests were performed using a universal testing machine at room temperature, and a stretching rate of $1.66 \times 10^{-3} \text{ s}^{-1}$ was used. The dimensions and the sampling location of the tensile test specimen are provided in Figure 3.

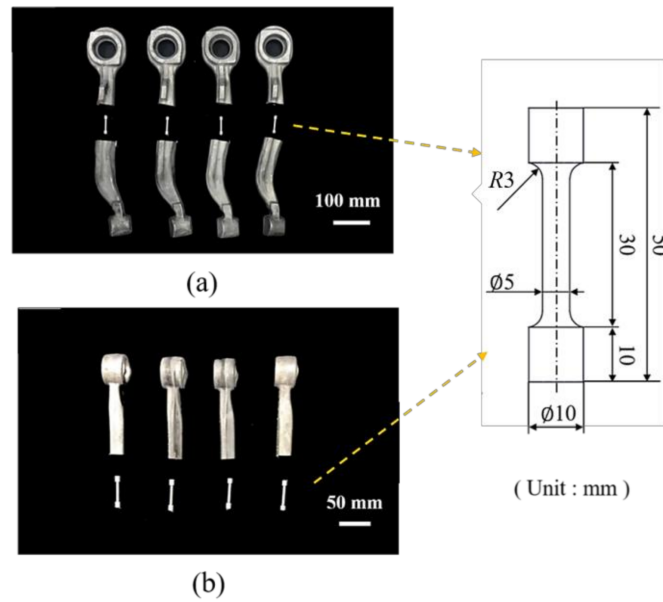


Figure 3. Sampling position and the specimen geometry of the tensile test: (a) L, (b) S.

The Young’s modulus was calculated from the relation in the Young’s region as follows: $E = \Delta\sigma / \Delta\epsilon$. This indicates that the Young’s modulus is equal to the ratio between changes in the stress in a specimen and its elongation. This relation is known as Hook’s law. All of the calculations were based on the data from the tensile test graph.

3. Results and Discussion

3.1. Hardness Values and Microstructural Observation

Figure 4 shows the hardness value for the L and S forgings after the heat treatments. It should be noted that the L forgings showed larger fluctuations than the S forgings, and according to the forming process, it is reasonable to suggest that the precipitate location makes a difference owing to the different deformation processes. However, the S forgings show smaller fluctuation than the L forgings because the S forgings experienced greater deformation levels during the forging process and became more uniform than the L forgings.

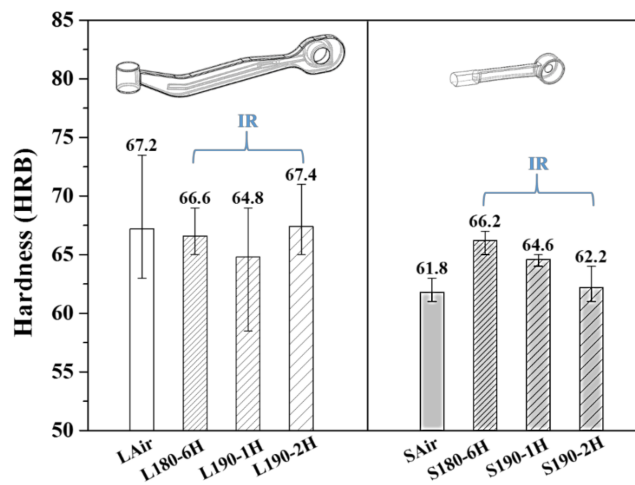


Figure 4. Hardness of the various heat-treated specimens.

In addition, the hardness of the L forgings after the IR heat treatment was similar to that of LAir, but the hardness of the S forgings after the IR heat treatment was higher than that of SAir. This indicates that 30 min of IR heat treatment can achieve the same solutionizing effect as that of the air furnace heat treatment. Moreover, the hardness of the L forgings and S forgings after the same IR heat treatment resulted in different hardness values, which could infer that the deformation during the forging process changed the material properties, which also means that the precipitation hardening behavior of the L forgings and S forgings was different even under the same IR heat treatment conditions. On the other hand, the fluctuations in the L190-1H became smaller with as the aging duration increased, and as is known from the discussion above, it can be suggested that under the L190-1H condition, the Mg and Si solute atoms are still in the process of precipitation and conversion.

Figure 5 demonstrates the grain size of the Al- α phase in the L forgings after the heat treatments. Both under the IR heat treatment condition and the air furnace heat treatment condition, significant dynamic recrystallization occurred in the matrix. These dynamic recrystallizations were formed during the forming process (extrusion and forging). To avoid the formation of coarse grains after the air furnace heat treatment, the solutionizing temperature was reduced (540 °C). However, equiaxial dynamic recrystallization grains and alignment in the remaining metal flows disappeared when the duration of the heat treatment was prolonged to 2 h. On the other hand, although the temperature used in the IR heat treatment process was higher than 540 °C (560 °C) for only 30 min, there was no evidence of coarse grains, and the dynamic recrystallization grains still aligned in the remaining metal flows after the IR heat treatment.

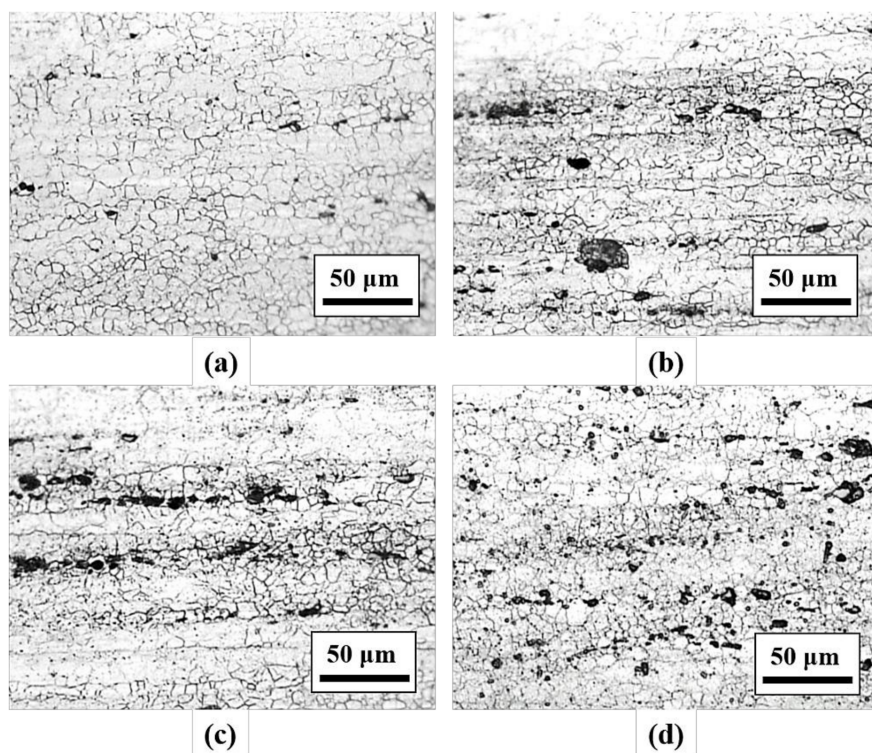


Figure 5. Metallographic images of the various heat-treated specimens: (a) LAir, (b) L180-6H, (c) L190-1H, (d) L190-2H.

Figure 6 demonstrates the grain size of the Al- α phase in the S forgings after the heat treatments. Both under the IR heat treatment condition and air furnace heat treatment condition, significant dynamic recrystallization occurred in the matrix. These dynamic recrystallizations were formed during the forming process (extrusion and forging), and no coarse grain formed. Furthermore, under both conditions, dynamic recrystallization grains aligned in the remaining metal flows. Comparing with

LAir, the SAir retention in the remaining metal flows occurred because SAir only solutionized for 1 h. Therefore, it could be inferred that with the solution treatment duration prolonged, non-equiaxed grains aligned in the remaining metal flows did not occur.

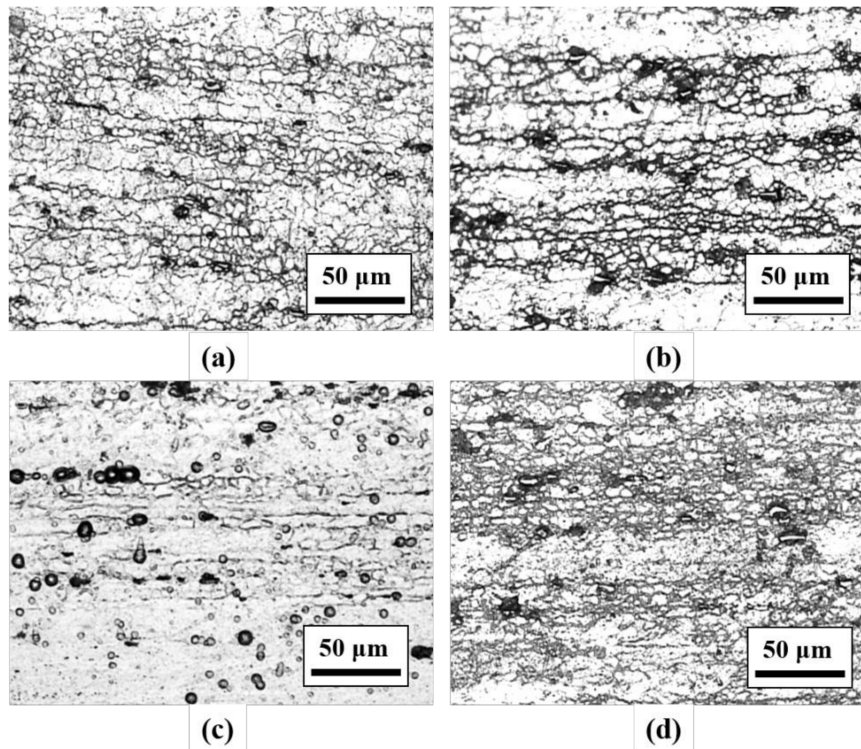


Figure 6. Metallographic images of the various heat-treated specimens: (a) SAir, (b) S180-6H, (c) S190-1H, (d) S190-2H.

Moreover, it has been reported that the occurrence of abnormal coarse grains is often due to the high temperature air furnace heat treatment [4] as well as the influence of fatigue properties [14]. In this study, although the IR heat treatment was performed at 560 °C, due to the efficiency of the high heat treatment, the heat treatment duration could be shortened, and therefore, no coarse grains developed.

Many black holes could be found on the specimens, as shown in Figures 5 and 6 compared with the non-corrosion specimens, these black holes were produced by the intermetallic compounds that preferentially eroded during the feature etching process. Figures 7 and 8 and Table 3 show the results of the SEM observation and EDS analysis focused on these intermetallic compounds.

Table 3. Energy dispersive spectrometer (EDS) analysis results for the examined specimen.

Forgings	L Forgings				S Forgings			
	Element at. %	A	B	C	D	E	F	G
Fe	2.52	4.67	5.86	5.76	4.79	7.01	6.62	8.17
Cu	0.47	0.68	0.38	0.49	1.14	1.42	1.37	1.63
Mg	1.60	0.88	0.55	1.01	1.71	1.18	0.91	1.31
Al	81.18	74.49	73.23	70.52	82.67	75.35	77.06	73.26
Si	6.53	9.55	11.24	9.65	5.65	7.91	7.86	8.46
Cr	2.42	2.66	1.98	3.43	0.75	0.87	0.70	1.16
Mn	5.28	7.07	6.76	9.14	3.29	6.25	5.48	6.01

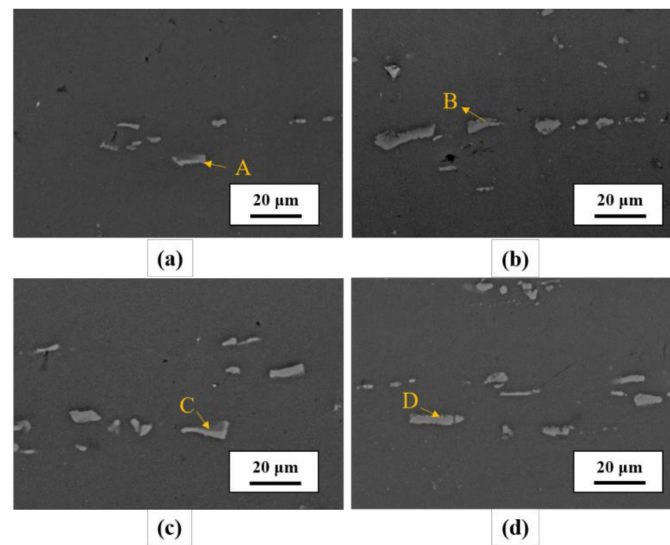


Figure 7. SEM observation results for the various heat-treated L forgings: (a) LAir, (b) L180-6H, (c) L190-1H, (d) L190-2H.

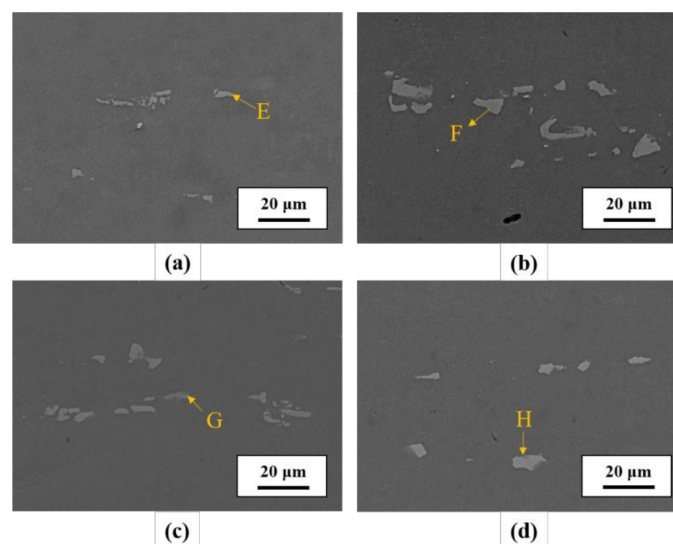


Figure 8. SEM observation results for the various heat-treated S forgings: (a) SAir, (b) S180-6H, (c) S190-1H, (d) S190-2H.

Figure 7 shows the results of the SEM observation of the L forgings, where many white intermetallic compounds could be found in the Al matrix. Based on the results of the EDS analysis focused on the intermetallic compounds, as provided in Table 3 (A, B, C, D), these white intermetallic compounds were Al(FeMnCr)Si phases. Previous reports have confirmed that the Al(FeMnCr)Si intermetallic compounds are the primary crystal phase formed during the casting process, and the relative content is changeable and stable at high temperatures. Thus, in this study, it is difficult to distinguish the specific composition of the Al(FeMnCr)Si phase and the Al(FeMnCr)Si intermetallic compounds remaining after the solution treatment process [5,15,16]. It should also be noted that these Al(FeMnCr)Si intermetallic compounds aligned the original extruded rod in the long axis direction. Previous studies have shown that these permutations may affect the grain size and Mg₂Si precipitation location [3].

Figure 8 shows the results of the SEM observation of the S forgings, where many white intermetallic compounds could be found in the Al matrix. From the results of the EDS analysis

focused on the intermetallic compounds, as provided in Table 3 (E, F, G, H), these white intermetallic compounds were Al(FeMnCr)Si phases. Al(FeMnCr)Si intermetallic compounds also obviously aligned along the long axis of the original extruded rod arrangement, but the smaller size as compared with the forming process suggests that the extruded bar used in the S forging forming process was slimmer (with a larger extruded ratio) than that in the L forging forming process.

The XRD results for the L and S forgings are shown in Figures 9 and 10, respectively. The results confirmed that the α -Al, Al(FeMnCr)Si, Mg_5Si_6 , and Mg_2Si phases existed. The Al(FeMnCr)Si phases were in agreement with the SEM and EDS analysis results. The Mg_2Si and Mg_5Si_6 were the strengthened phases that formed during the aging process [4,17,18]. And this matches the result of hardness (Figure 4) and the tensile strength discussed in the next section.

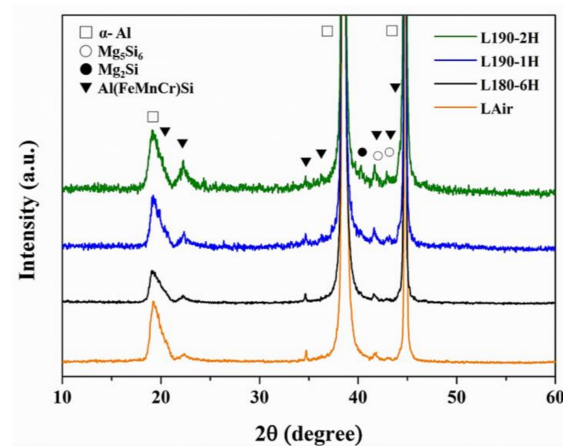


Figure 9. X-ray diffraction patterns of L forgings for the different heat treatment states.

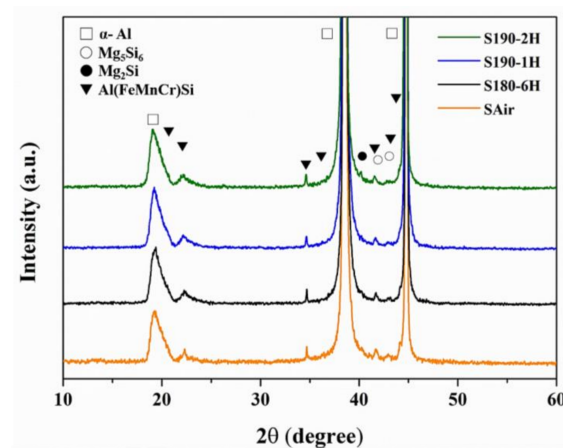


Figure 10. X-ray diffraction patterns of S forgings for the different heat treatment states.

3.2. Tensile Mechanical Properties and Fracture Observation

Figures 11 and 12 and Table 4 show the results of the tensile test, indicating that the tensile strength and the tensile elongation were better than commercial 6082 forgings (Tensile strength: * 1 (Ultimate tensile strength, UTS); * 2 (Yield strength, YS) ; Tensile ductility: * 3 (Total elongation, TE) [19,20]). Comparing the effect of heat treatment on the L forgings, L180-6H achieved similar tensile properties to those of LAir. When the aging temperature was increased to 190 °C, and the aging duration was prolonged to 2 h, the tensile strength and the tensile elongation of L190-2H were better than either LAir or L180-6H. A comparison of the effect of heat treatment on the S forgings indicated that the tensile strength of S180-6H was less than that of SAir, but similar elongation was achieved. After increasing

the artificial aging temperature and duration (S190-2H), the tensile strength and elongation was better than that of S180-6H and S190-1H.

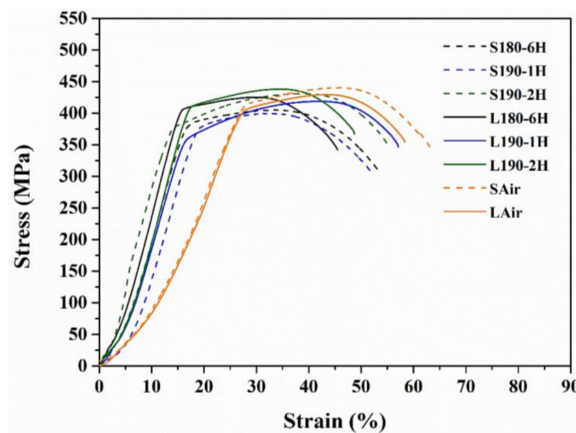


Figure 11. Stress-strain forging curves for the different heat treatment states.

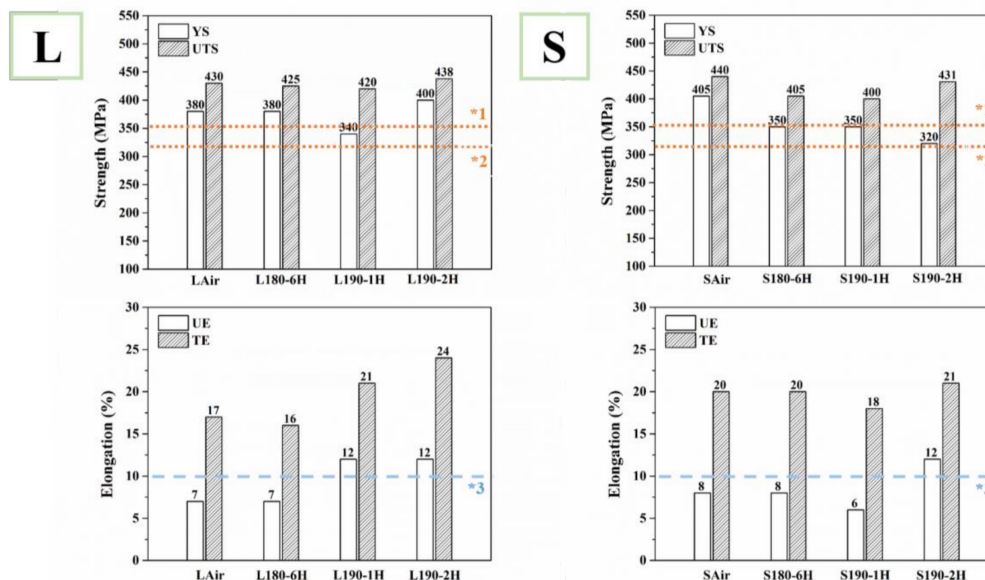


Figure 12. Specific properties of Figure 11 and Table 4 (* 1 (Ultimate tensile strength, UTS), * 2 Yield strength, YS): data from Ref. [19], * 3 (Total elongation, TE): data from Ref. [20]).

Table 4. Specific tensile strength and elongation values of Figure 11 (L: L forgings, S: S forging).

Sample	Yield Strength (MPa)	Ultimate Tensile Strength (MPa)	Uniform Elongation (%)	Total Elongation (%)
LAir	380	430	7	17
L180-6H	380	425	7	16
L190-1H	340	419	12	21
L190-2H	400	438	12	24
SAir	405	440	8	20
S180-6H	350	405	8	20
S190-1H	350	400	6	18
S190-2H	320	431	12	21

Figures 13a–d and 14a–d demonstrate the fracture surface of the specimens after the tensile test. Dimples could be observed on both the L and S forgings specimens, which means that the fracture of

the material was caused by microvoid coalescence. Microvoid coalescence proceeds in three stages: nucleation, growth, and coalescence of microvoids. For 6082 aluminum alloys, the nucleation site of microvoids often occurs between the intermetallic compounds (or precipitate particles) and the matrix. In this study, Al(FeMnCr)Si intermetallic compounds could be found in large dimples. In the case of the small dimples, based upon research and the XRD results, it could be concluded that the small dimples were caused by the fine Al(FeMnCr)Si phase and precipitates (Mg_5Si_6 and Mg_2Si) [3,15].

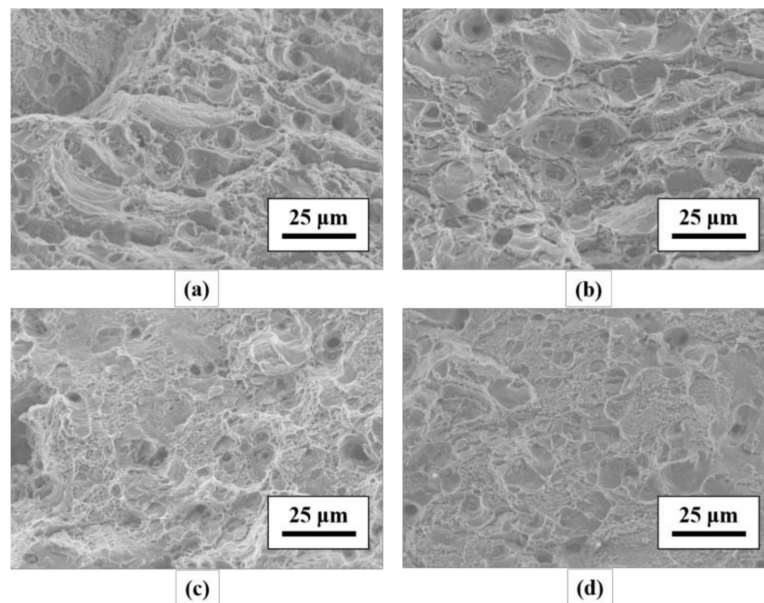


Figure 13. Fracture surface of the L forgings after the tensile test: (a) LAir, (b) L180-6H, (c) L190-1H, (d) L190-2H.

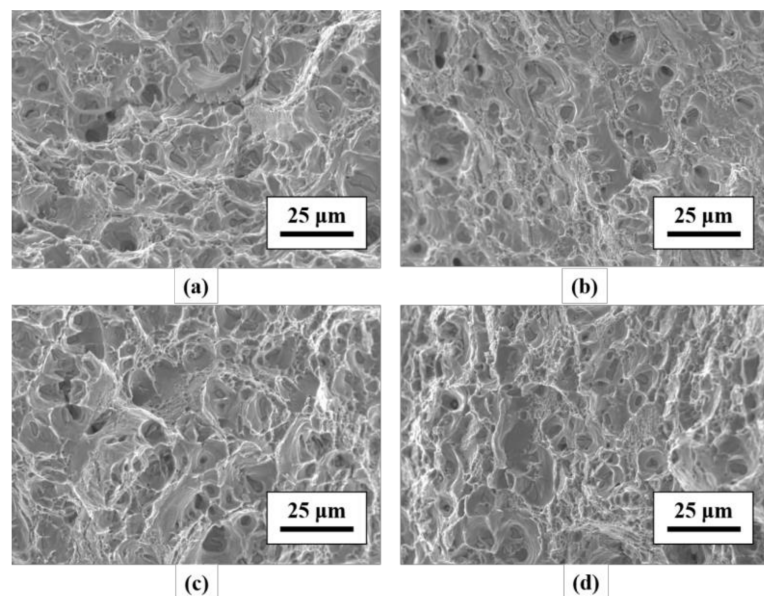


Figure 14. Fracture surface of the S forgings after the tensile test: (a) SAir, (b) S180-6H, (c) S190-1H, (d) S190-2H.

In addition, the dimples on the LAir specimen were more uniform in size than the dimples on the L180-6H, L190-1H, and L190-2H specimens. According to a previous report [21], a fracture occurs

due to incorporated dimples, where the mixed dimple sizes delay dimple linkage. When the dimple linkage is delayed, the elongation property of the material is increased, which is consistent with the results shown in Figure 12. However, the dimple size was effect by the second phases and the grain size of the matrix. Grain sizes in the S forgings were similar; hence, it was difficult to observe the obvious differences between the fracture surface of the S forgings.

3.3. Young's Modulus Rise Effect

Figure 11 and Table 5 show the Young's modulus of the strain-stress curves, where using the IR heat treatment, the Young's modulus of the L forgings increased by 30–45.3%, and the Young's modulus of the S forgings increased by 32.6–42.9%.

Table 5. Young's modulus of the forgings after heat treatment. (↑: went up by).

Sample	Young's Modulus σ/ϵ (GPa)	Comparison with Air Furnace Heat Treatment Specimens
LAir	22.3	-
L180-6H	32.4	↑45.3%
L190-1H	29.0	↑30.0%
L190-2H	32.2	↑44.4%
SAir	21.9	-
S180-6H	31.3	↑42.9%
S190-1H	29.1	↑32.6%
S190-2H	29.7	↑35.6%

Young's modulus is associated with the lattice distance and the bonding forces of atoms, where a higher Young's modulus allows a material to have greater resistance during the Young's deformation. Based on previous research [14], the Young's modulus of a 6082 aluminum alloy is strongly influenced by precipitates. Our previous work revealed that a solution heat treatment with a faster heating rate can increase the magnesium content in the Mg, Si precipitates [12]; hence, it can be inferred that the increment in the Young's modulus in this study is due to differences the in Mg, Si solute content and precipitates.

The mechanical properties and microstructure of the L and S forgings after different heat treatment processes are plotted in Figure 15. Firstly, different masses of the 6082 aluminum forgings after air furnace heat treatment show different Young's modulus values and elongation. Secondly, the IR heat treatment was shown to increase the Young's modulus and the elongation of the 6082 aluminum forgings, where the grain still aligned in the remaining metal flows. In addition, the total heat treatment duration could be reduced.

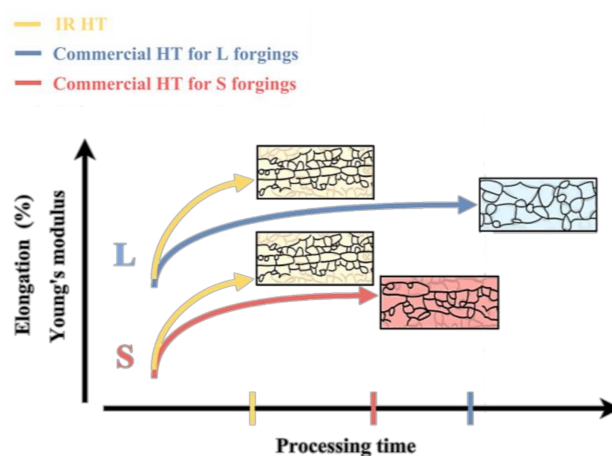


Figure 15. A schematic diagram of the mechanical properties and microstructures in the different heat treatment processes.

4. Conclusions

In this study, the superiority and the feasibility of an IR heat treatment was investigated. The following findings were obtained:

1. The variability in the mechanical properties of L and S primarily affected by different forging processes can be reduced through an IR heat treatment. An air furnace heat treatment can't achieve the same results.
2. For IR heat treatment specimens, the best IR heat treatment condition for L and S forging is a solution heat treatment for 30 min at 560 °C and artificial aging for 2 h at 190 °C. The tensile strength was shown to be similar to that of the air furnace heat treated specimens, and the non-equiaxed grains remained aligned in the remaining metal flows, which enhanced the elongation.
3. Using an IR heat treatment can curtail the duration of the heat treatment, which showed a striking benefit, according to the Young's modulus. The Young's modulus values for the IR heat treatment specimens were higher than those for the air furnace heat treatment.

Acknowledgments: The authors are grateful to the Instrument Center of National Cheng Kung University and the Ministry of Science and Technology, Taiwan (Grant No. MOST 106-2221-E-006-064) for their financial support. All sources of funding of the study should be disclosed. Please clearly indicate grants that you have received in support of your research work. Clearly state if you received funds for covering the costs to publish in open access.

Author Contributions: Yi-Ling Chang performed the experiments, analyzed the data, and wrote the paper. Fei-Yi Hung and Truan-Sheng Lui are advisers.

Conflicts of Interest: The authors declare no conflict of interest.

References

1. Das, S.K. Designing aluminium alloys for a recycling friendly world. *Mater. Sci. Forum* **2006**, *519*, 1239–1244. [[CrossRef](#)]
2. Birol, Y.; Ilgaz, O. Effect of cast and extruded stock on grain structure of EN AW 6082 alloy forgings. *Mater. Sci. Technol.* **2014**, *30*, 860–866. [[CrossRef](#)]
3. Birol, Y.; Gokcil, E. Processing of high strength EN AW 6082 forgings without a solution heat treatment. *Mater. Sci. Eng. A-Struct. Mater.* **2016**, *674*, 25–32. [[CrossRef](#)]
4. Birol, Y. Effect of extrusion press exit temperature and chromium on grain structure of EN AW 6082 alloy forgings. *Mater. Sci. Technol.* **2015**, *31*, 207–211. [[CrossRef](#)]
5. Mrówka-Nowotnik, G.; Sieniawski, J. Influence of heat treatment on the microstructure and mechanical properties of 6005 and 6082 aluminium alloys. *J. Mater. Process. Technol.* **2005**, *162*, 367–372. [[CrossRef](#)]
6. Vamadevan, G.; Kraft, F. Application of Rapid Infrared Heating for Processing of Aluminum Forgings. In *The James Morris Honorary Symposium on Aluminum Wrought Products for Automotive, Packing, and Other Applications*; The Minerals, Metals & Materials Society: Santa Barbara, CA, USA, 2006.
7. Kervick, R.; Blue, C. *Enhancement of Aluminum Alloy Forgings through Rapid Billet Heating*; KomTeK: Worcester, MA, USA, 2006.
8. Lu, H.; Kadolkar, P.B. Control of Grain Size and Age Hardening in AA2618 Forgings Processed by Rapid Infrared Radiant Heating. *TMS Lett.* **2004**, *1*, 47–48.
9. Chang, Y.L.; Hung, F.Y. Study of microstructure and tensile properties of infrared-heat-treated cast-forged 6082 aluminum alloy. *JMRT* **2017**, in press. [[CrossRef](#)]
10. Xie, C.; Schaller, R. High damping capacity after precipitation in some commercial aluminum alloys. *Mater. Sci. Eng. A-Struct. Mater.* **1998**, *252*, 78–84. [[CrossRef](#)]
11. Reeb, A.; Merzkirch, M. Heat treatment during composite extruded spring steel wire reinforced EN AW-6082. *J. Mater. Process. Technol.* **2016**, *229*, 1–8. [[CrossRef](#)]
12. Chang, Y.L.; Hung, F.Y. Enhancing the tensile yield strength of A6082 aluminum alloy with rapid heat solutionizing. *Mater. Sci. Eng. A-Struct. Mater.* **2017**, *702*, 438–445. [[CrossRef](#)]
13. Birol, Y. The effect of processing and Mn content on the T5 and T6 properties of AA6082 profiles. *J. Mater. Process. Technol.* **2006**, *173*, 84–91. [[CrossRef](#)]

14. Birol, Y.; Ilgaz, O. Comparison of cast and extruded stock for the forging of AA6082 alloy suspension parts. *Adv. Mater. Res.* **2014**, *939*, 299–304. [[CrossRef](#)]
15. Mrówka-Nowotnik, G.; Sieniawski, J. Effect of heat treatment on tensile and fracture toughness properties of 6082 alloy. *J. Achieve Mater. Manuf. Eng.* **2009**, *32*, 162–170.
16. Meredith, M.; Worth, J. Intermetallic phase selection during solidification of Al-Fe-Si (-Mg) alloys. In *Mater Sci Forum*; Trans Tech Publications: Zürich, Switzerland, 2002; Volume 107–112.
17. Brito, C.; Costa, T.A. Characterization of dendritic microstructure, intermetallic phases, and hardness of directionally solidified Al-Mg and Al-Mg-Si alloys. *Metall. Mater. Trans. A* **2015**, *46*, 3342–3355. [[CrossRef](#)]
18. Birol, Y. Effect of cooling rate on precipitation during homogenization cooling in an excess silicon AlMgSi alloy. *Mater. Charact.* **2012**, *73*, 37–42. [[CrossRef](#)]
19. Santos, J.; Gouveia, R.M. Designing a new sustainable approach to the change for lightweight materials in structural components used in truck industry. *J. Clean. Prod.* **2017**, *164*, 115–123. [[CrossRef](#)]
20. Nakamura, H.; Nishibata, M. Globalization of Aluminum Forging Automotive Suspension Business: Establishment of Production Bases in Japan, USA and China. *“R&D” Kobe Steel Eng. Rep.* **2017**, *66*, 99–102.
21. Hosoda, N.; Nakai, M. The Effect of Microstructure on Mechanical Properties of Forged 6061 Aluminum Alloy. *Mater. Forum* **2004**, *28*, 1382–1387.



© 2018 by the authors. Licensee MDPI, Basel, Switzerland. This article is an open access article distributed under the terms and conditions of the Creative Commons Attribution (CC BY) license (<http://creativecommons.org/licenses/by/4.0/>).